Article

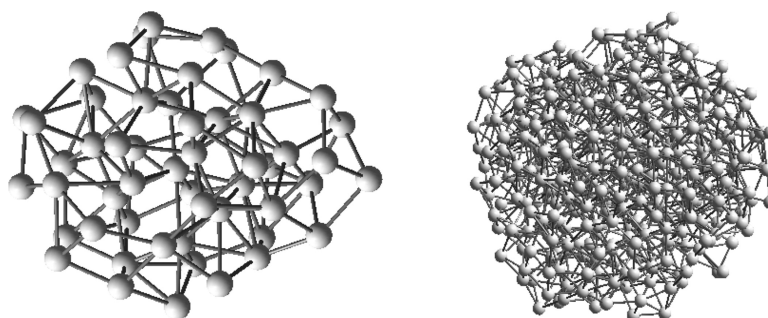# Nanosolids, Slushes, and Nanoliquids: Characterization of Nanophases in Metal Clusters and Nanoparticles

Zhen Hua Li, and Donald G. Truhlar

More About This Article

Additional resources and features associated with this article are available within the HTML version:

- Supporting Information
- Access to high resolution figures
- Links to articles and content related to this article
- Copyright permission to reproduce figures and/or text from this article

View the Full Text HTML

Nanosolids, Slushes, and Nanoliquids: Characterization of Nanophases in Metal Clusters and Nanoparticles

Zhen Hua Li*,† and Donald G. Truhlar*,‡

Department of Chemistry, Fudan University, Shanghai, 200433, China and Department of Chemistry and Supercomputing Institute, University of Minnesota, Minneapolis, Minnesota 55455-0431

Received April 3, 2008; E-mail: lizhenhua@fudan.edu.cn; truhlar@umn.edu

Abstract: One of the keys to understanding the emergent behavior of complex materials and nanoparticles is understanding their phases. Understanding the phases of nanomaterials involves new concepts not present in bulk materials; for example, the phases of nanoparticles are quantum mechanical even when no hydrogen or helium is present. To understand these phases better, molecular dynamics (MD) simulations on size-selected particles employing a realistic analytic many-body potential based on quantum mechanical nanoparticle calculations have been performed to study the temperature-dependent properties and melting transitions of free Al_n clusters and nanoparticles with $n = 10-300$ from 200 to 1700 K. By analyzing properties of the particles such as specific heat capacity (c), radius of gyration, volume, coefficient of thermal expansion (β), and isothermal compressibility (κ), we developed operational definitions of the solid, slush, and liquid states of metal clusters and nanoparticles. Applying the definitions, which are based on the temperature dependences of c, β, and $\ln \kappa$, we determined the temperature domains of the solid, slush, and liquid states of the Al_n particles. The results show that Al_n clusters ($n \leq 18$, diameter of less than 1 nm) are more like molecules, and it is more appropriate to say that they have no melting transition, but Al_n nanoparticles ($n \geq 19$, diameter of more than 1 nm) do have a melting transition and are in the liquid state above $900-1000$ K. However, all aluminum nanoparticles have a wide temperature interval corresponding to the slush state in which the solid and liquid states coexist in equilibrium, unlike a bulk material where coexistence occurs only at a single temperature (for a given pressure). The commonly accepted operational marker of the melting temperature, namely, the peak position of c, is not unambiguous and not appropriate for characterizing the melting transition for aluminum particles with the exception of a few particle sizes that have a single sharp peak (as a function of temperature) in each of the three properties, c, β, and $\ln \kappa$.

1. Introduction

Metal clusters and nanoparticles, as an intermediate form of matter[1−7] between the composing atoms and the corresponding bulk materials, have distinct electrical, optical, magnetic, chemical, and catalytic properties and have been the subjects of extensive experimental and theoretical study. Understanding the evolution of various physical and chemical properties from the atomic to the bulk limit is also of great fundamental and practical interest. Often, when we face a new class of phenomena we "borrow" concepts from well-studied ones. However, one must be careful when applying macroconcepts to finite systems because these concepts may be ill defined for finite systems. For example, melting is well defined on the macroscale but not on the nanoscale.[8−13] Molecular dynamics simulations of metal nanoparticles have uncovered dynamic phase coexistence phenomena not present in bulk metals.[14−19]

Understanding the molecular thermodynamics of nanophases is a key enabler for the bottom-up approach to nanodesign. For macroscopic systems, a phase is a state with uniform[20] or continuously varying[21] physical and chemical properties (intensive thermodynamic variables) in a well-defined temperature and pressure range. The change from one phase to another phase

† Fudan University.
‡ University of Minnesota.
(1) Bonacic-Koutecky, V.; Fantucci, P.; Koutecky, J. *Chem. Rev.* **1991**, *91*, 1035. de Heer, W. A. *Rev. Mod. Phys.* **1993**, *65*, 611.
(2) Feldheim, D. L.; Foss, C. A. *Metal Nanoparticles: Synthesis, Characterization, and Applications*; Marcel Dekker: New York, 2002.
(3) Buchachenko, A. L. *Russ. Chem. Rev.* **2003**, *72*, 375.
(4) Schmid, G. *Nanoparticles: From Theory to Applications*; Wiley-VCH: Weinheim, 2004.
(5) Chan, K.-Y.; Ding, J.; Ren, J.; Cheng, S.; Tsang, K. Y. *J. Mater. Chem.* **2004**, *14*, 505. Heiz, U.; Bullock, E. L. *J. Mater. Chem.* **2004**, *14*, 564. O'Hair, R. A. J.; Khairallah, G. N. *J. Cluster Sci.* **2004**, *15*, 331.
(6) Baletto, F.; Ferrando, R. *Rev. Mod. Phys.* **2005**, *77*, 371.
(7) Astruc, D.; Lu, F.; Aranzaes, T. R. *Angew. Chem., Int. Ed.* **2005**, *44*, 7852. Watanabe, K.; Menzel, P.; Nilius, N.; Freund, H.-J. *Chem. Rev.* **2006**, *106*, 4301. Perepichka, D. F.; Rosei, F. *Angew. Chem., Int. Ed.* **2007**, *46*, 6006. Jellinek, J. *Faraday Discuss.* **2008**, *138*, 11.

(8) Berry, R. S.; Jellinek, J.; Natanson, G. *Phys. Rev. A* **1984**, *30*, 919.
(9) Beck, T. L.; Jellinek, J.; Berry, R. S. *J. Chem. Phys.* **1987**, *87*, 545.
(10) Berry, R. S.; Wales, D. J. *Phys. Rev. Lett.* **1989**, *63*, 1156. (a) Wales, D. J.; Berry, R. S. *J. Chem. Phys.* **1990**, *92*, 4473. Berry, R. S. *J. Chem. Soc., Faraday Trans.* **1990**, *86*, 2343. Berry, R. S. *Sci. Am.* **1990**, *263*, 68.
(11) Berry, R. S. In *Clusters of Atoms and Molecules*; Haberland, H., Ed.; Springer Series in Chemical Physics 52; Springer: Berlin, 1994; p 187. Berry, R. S. *Microscale Thermophys. Eng.* **1997**, *1*, 1. Proykova, A.; Berry, R. S. *J. Phys. B: At. Mol. Opt. Phys.* **2006**, *39*, R167.
(12) Berry, R. S. *C. R. Phys.* **2002**, *3*, 319.
(13) Schmidt, M.; Haberland, H. *C. R. Phys.* **2002**, *3*, 327.

under equilibrium conditions usually occurs in a very narrow temperature and pressure range (spontaneously). A small change in temperature or pressure completely changes the phase from one to the other. Thus, the change of phase can be characterized by a transition temperature T_{tran}. However, for clusters and nanoparticles ranging in size from several atoms to thousands of atoms, the transition from one equilibrium phase to another equilibrium phase occurs gradually in a wider temperature range.[6,11,12,22,23] Within this range the two phases are in equilibrium with each other. Therefore, the phase change in finite systems has to be characterized by two temperatures, T_1 and T_2 with $T_2 > T_1$.[8-10,12] Below T_1, the amount of phase 2 is negligible, while above T_2, the amount of phase 1 is negligible. For a solid−liquid transition, T_1 is the freezing temperature T_f and T_2 is the melting temperature T_m. Between the two temperatures is the solid−liquid coexistence region.[14-19] For macroscopic systems under equilibrium conditions, $T_f = T_m$.[8,10,20,21]

Experimentally, one convenient way to study a melting transition is to measure the caloric curve (energy as a function of temperature) of the system.[13] The heat capacity is the derivative of the caloric curve. Caloric curves have been used to study the melting of clusters and nanoparticles,[6,13,24-44] both experimentally and theoretically, as well as bulk materials. For some cases, the heat capacity curve has a sharp peak, but for
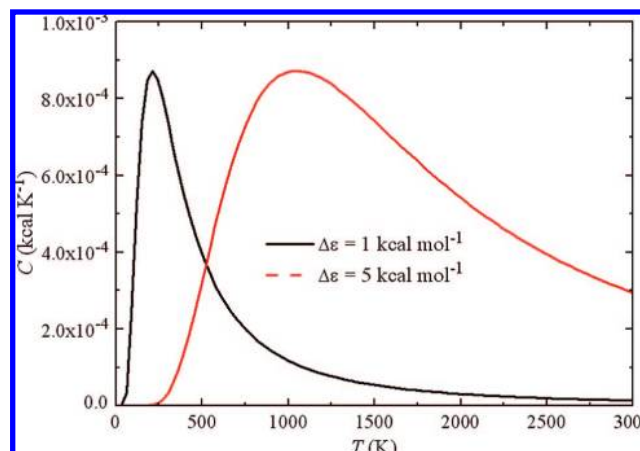

Figure 1. Heat capacity of a model system with two nondegenerate states.

others it does not.[26,32,35,36,38,42-44] Usually, as in macroscopic systems,[21] the former case has been called a first-order melting transition while the latter has often been called a second-order melting transition,[35] although there are also second-order phase transitions of other kinds in bulk materials.

The temperature at which the heat capacity curve has a peak or maximum will be called the peak temperature (T_p) of the heat capacity. Although the melting temperature is usually taken as this peak temperature, this is not necessarily a valid procedure for finite systems. Consider a model system with only two states, both nondegenerate, which may be two electronic states or two isomers in equilibrium with each other; the partition function of the system is

$$Q = 1 + e^{-\Delta\varepsilon/k_B T} \tag{1}$$

where $\Delta\varepsilon$ is the energy gap between the two states. Then the heat capacity of the system is

$$C = \frac{\Delta\varepsilon^2/k_B T^2}{(e^{\Delta\varepsilon/2k_B T} + e^{-\Delta\varepsilon/2k_B T})^2} \tag{2}$$

Plots of C vs T with two different values of $\Delta\varepsilon$ are depicted in Figure 1. Since the two states involved can be any two states, not necessarily a liquid and a solid state, it is clear that observing a peak in the C curve is not enough to indicate a melting transition. It may just result from equilibrium between two electronic states or two structural isomers with different energies. Moreover, it is easy to show that at T_p the population of the higher energy state is just 13% ($e^{-2}/(1 + e^{-2})$). Therefore, even if one can call this a melting transition, it is questionable whether the temperature at which C has a peak should be called the melting temperature since the majority of the system can still be in the solid state. In a strict sense, since the transition is gradual, there is no melting *point* at all. Since clusters and

(14) Vichare, A.; Kanhere, D. G. *J. Phys: Condens. Matter* **1998**, *10*, 3309.
(15) Cleveland, C. L.; Luedtke, W. D.; Landman, U. *Phys. Rev. B* **1999**, *60*, 5065.
(16) Pochon, S.; MacDonald, K. F.; Knize, R. J.; Zheludev, N. I. *Phys. Rev. Lett.* **2004**, *92*, 145702.
(17) Schebarchov, D.; Hendy, S. C. *J. Chem. Phys.* **2006**, *123*, 104701.
(18) Schebarchov, D.; Hendy, S. C. *Phys. Rev. B* **2006**, *73*, 121402(R).
(19) Alavi, S.; Thompson, D. L. *J. Phys. Chem. A* **2006**, *110*, 1518.
(20) Atkins, P.; Paula, J. D. *Atkins' Physical Chemistry*, 7th ed.; Oxford University Press: New York, 2002; p 135.
(21) Berry, R. S.; Rice, S. A.; Ross, J. *Physical Chemistry*, 2nd ed.; Topics in Physical Chemistry Series 12; Oxford University Press: New York, 2000; pp 397,658. See also p 347.
(22) Sebetci, A.; Güvenc, Z. B.; Kökten, H. *Comput. Mater. Sci.* **2006**, *35*, 152.
(23) Rodumer, E. *Chem. Soc. Rev.* **2006**, *35*, 583.
(24) Rey, C.; Gallego, L. J.; Garcı́a-Rodeja, J.; Alonso, J. A.; Iñiguez, M. P. *Phys. Rev. B* **1993**, *48*, 8253.
(25) Nayak, S. K.; Khanna, S. N.; Rao, B. K.; Jena, P. *J. Phys.: Condens. Matter* **1998**, *10*, 10853.
(26) Schmidt, M.; Kusche, R.; Kronmüler, W.; von Issendorff, B.; Haberland, H. *Phys. Rev. Lett.* **1997**, *79*, 99. Schmidt, M.; Kusche, R.; von Issendorff, B.; Haberland, H. *Nature* **1998**, *393*, 238.
(27) Sun, D. Y.; Gong, X. G. *Phys. Rev. B* **1998**, *57*, 4730.
(28) Efremov, M. Yu.; Schiettekatte, F.; Zhang, M.; Olson, E. A.; Kwan, A. T.; Berry, R. S.; Allen, L. H. *Phys. Rev. Lett.* **2000**, *85*, 3560.
(29) Jellinek, J.; Goldberg, A. *J. Chem. Phys.* **2000**, *113*, 2570.
(30) Schmidt, M.; Hippler, Th.; Donges, J.; Kronmüller, W.; von Issendorff, B.; Haberland, H.; Labastie, P. *Phys. Rev. Lett.* **2001**, *87*, 203402. Schmidt, M.; Donges, J.; Hippler, Th.; Haberland, H. *Phys. Rev. Lett.* **2003**, *90*, 103401.
(31) Breaux, G. A.; Benirschke, R. C.; Sugai, T.; Kinnear, B. S.; Jarrold, M. F. *Phys. Rev. Lett.* **2003**, *91*, 215508.
(32) Breaux, G. A.; Hillman, D. A.; Neal, C. M.; Benirschke, R. C.; Jarrold, M. F. *J. Am. Chem. Soc.* **2004**, *126*, 8628.
(33) Lai, S. K.; Lin, W. D.; Wu, K. L.; Li, W. H.; Lee, K. C. *J. Chem. Phys.* **2004**, *121*, 1487.
(34) Werner, R. *Eur. Phys. J. B* **2005**, *43*, 47.
(35) Breaux, G. A.; Cao, B.; Jarrold, M. F. *J. Phys. Chem. B* **2005**, *109*, 16575.
(36) Breaux, G. A.; Neal, C. M.; Cao, B.; Jarrold, M. F. *Phys. Rev. Lett.* **2005**, *94*, 173401.
(37) de Bas, B. S.; Ford, M. J.; Cortie, M. B. *J. Phys.: Condens. Matter* **2006**, *18*, 55.
(38) Joshi, K.; Krishnamurty, S.; Kanhere, D. G. *Phys. Rev. Lett.* **2006**, *96*, 135703.
(39) Noya, E. G.; Doye, J. P. K.; Calvo, F. *Phys. Rev. B* **2006**, *73*, 125407.

(40) Zhang, W.; Zhang, F. S.; Zhu, Z. Y. *Phys. Rev. B* **2006**, *74*, 033412. Zhang, W.; Zhang, F. S.; Zhu, Z. Y. *Eur. Phys. J. D* **2007**, *43*, 97. Zhang, W.; Zhang, F. S.; Zhu, Z. Y. *Chin. Phys. Lett.* **2007**, *24*, 1915.
(41) Duan, H. M.; Ding, F.; Rosen, A.; Harutyunyan, A. R.; Curtarolo, S.; Bolton, K. *Chem. Phys.* **2007**, *333*, 57.
(42) Neal, C. M.; Starace, A. K.; Jarrold, M. F. *J. Am. Soc. Mass Spectrom.* **2007**, *18*, 74.
(43) Neal, C. M.; Starace, A. K.; Jarrold, M. F.; Joshi, K.; Krishnamurty, S.; Kanhere, D. G. *J. Phys. Chem. C* **2007**, *111*, 17788.
(44) Neal, C. M.; Atarace, A. K.; Jarrold, M. F. *Phys. Rev. B* **2007**, *76*, 54113.

nanoparticles are often a mixture of many isomers with similar energies equilibrating with each other,[6,18,22,23,29,37,45–48] their melting transitions have the same ambiguity.

The distinction between clusters and nanoparticles is not strict, and we use the generic name particles to refer to both of them. Aluminum particles have been of great experimental[36,42–44,49–56] and theoretical[14,19,27,29,33,34,39,40,43,57–86] interest for decades.

Their melting has recently been the subject of extensive experimental[36,42–44] and theoretical study.[14,19,27,33,34,40,82–86] Jarrold et al. used multicollision-induced dissociation to measure the heat capacities of Al_n cationic clusters with $n = 16$–48,[44] 31–38,[43] 49–63,[36] and 63–83.[42] They found that for some clusters the heat capacity curve has a well-defined sharp peak, while for others the heat capacity curve is relatively flat and featureless. Taking the temperature T_p at which C has a maximum as the melting temperature, they found that the melting temperature depends greatly on particle size, and even a change in size by a single atom can make huge differences. Monte Carlo[34,39] (MC) and molecular dynamics[14,19,27,33,40,83,84] (MD) simulations confirmed the experimental findings. However, T_p is not enough to characterize a melting transition since the solid and liquid states in finite systems have not been well defined. Moreover, for those particles with featureless and flat heat capacity curves, T_p has large uncertainties and should be treated with caution.[44]

For the particle sizes studied here, most atoms need to be classified as surface atoms rather than as interior atoms with bulk properties characteristic of a macroscopic particle. Except for a few small clusters, Al_{13},[14] Al_{13}^-,[83] and Al_{14},[83] available simulations of Al cluster melting all use empirical analytical potential functions, but it is not possible to accurately parametrize empirical potentials in the cluster and nanoparticle regime due to a lack of experimental data for systems with a significant fraction of atoms in nonbulk (e.g., surface) positions.[24,87] Recently, economical and accurate analytic potentials for aluminum systems have been developed by fitting to results of well-validated electronic-structure calculations[78] for Al_n clusters and nanoparticles as well as to experimental bulk properties.[88] Because pairwise additive potentials are inaccurate for real metals, including metal clusters and metal nanoparticles, these analytic potentials include many-body effects (i.e., the potentials are not pairwise additive). The many-body (nonpairwise, NP) potentials named NP-A and NP-B are the most accurate potentials available for aluminum systems[88] or any metal nanoparticles. The potentials have been successfully applied to aluminum systems to study the vapor–liquid coexistence of Al,[89] energy landscape,[48] thermodynamics properties,[81] and reactions[90] of Al_n particles. Here we use the NP-B potential to study melting, if we can call it that, of Al_n particles with $n = 10$–300, which have diameters in the range of about 0.8–2.5 nm.

For convenience we call the particles with a diameter less than ~1 nm clusters and those with diameters larger than ~1 nm nanoparticles. For aluminum particles, Al_{19} has a diameter of about 1 nm.[88,91] Thus, Al_n particles with $n \leq 18$ will be called clusters, and those with $n \geq 19$ will be called nanoparticles. In the present study, by analyzing simulation results, we

(45) Doye, J. P. K.; Calvo, F. *Phys. Rev. Lett.* **2001**, *86*, 3570. Doye, J. P. K.; Calvo, F. *J. Chem. Phys.* **2003**, *119*, 12680.

(46) Wang, G. M.; Blaisten-Barojas, E.; Roitberg, A. E. *J. Chem. Phys.* **2001**, *115*, 3640.

(47) Baletto, F.; Rapallo, A.; Rossi, G.; Ferrando, R. *Phys. Rev. B* **2004**, *69*, 235421. Rossi, G.; Rapallo, A.; Mottet, C.; Fortunelli, A.; Baletto, F.; Ferrando, R. *Phys. Rev. Lett.* **2004**, *93*, 105503.

(48) Li, Z. H.; Jasper, A. W.; Truhlar, D. G. *J. Am. Chem. Soc.* **2007**, *129*, 14899.

(49) de Heer, W. A.; Milani, P.; Chatelain, A. *Phys. Rev. Lett.* **1989**, *63*, 2834.

(50) Lermé, J.; Pellarin, M.; Vialle, J. L.; Baguenard, B.; Broyer, M. *Phys. Rev. Lett.* **1992**, *68*, 2818. Baguenard, B.; Pellarin, M.; Lermé, J.; Vialle, J. L.; Broyer, M. *J. Chem. Phys.* **1994**, *100*, 754.

(51) Martin, T. P.; Näher, U.; Schaber, H. *Chem. Phys. Lett.* **1992**, *199*, 470.

(52) Jarrold, M. F.; Bower, J. E. *J. Phys. Chem.* **1993**, *97*, 1746. Jarrold, M. F.; Bower, J. E. *J. Chem. Phys.* **1993**, *98*, 2399. Jarrold, M. F. *J. Phys. Chem.* **1995**, *99*, 11.

(53) Cha, C. Y.; Ganteför, G.; Eberhardt, W. *J. Chem. Phys.* **1994**, *100*, 995. Ganteför, G.; Eberhardt, W. *Chem. Phys. Lett.* **1994**, *217*, 600.

(54) Li, X.; Wu, H.; Wang, X. B.; Wang, L. S. *Phys. Rev. Lett.* **1998**, *81*, 1909.

(55) Akola, J.; Manninen, M.; Hakkinen, H.; Landman, U.; Li, X.; Wang, L. S. *Phys. Rev. B* **1999**, *60*, 11297. Akola, J.; Manninen, M.; Hakkinen, H.; Landman, U.; Li, X.; Wang, L. S. *Phys. Rev. B* **2000**, *62*, 13216. Kuznetsov, A. E.; Boldyrev, A. I.; Zhai, H. J.; Li, X.; Wang, L. S. *J. Am. Chem. Soc.* **2002**, *124*, 111791.

(56) Schnepf, A.; Schnöckel, H. *Angew. Chem., Int. Ed.* **2002**, *41*, 3532.

(57) Jones, R. O. *Phys. Rev. Lett.* **1991**, *67*, 224. Jones, R. O. *J. Chem. Phys.* **1993**, *99*, 1194.

(58) Cheng, H.-P.; Berry, R. S.; Whetten, R. L. *Phys. Rev. B* **1991**, *43*, 10647.

(59) Yi, J. Y.; Oh, D. J. U.; Bernholc, J. *Phys. Rev. Lett.* **1991**, *67*, 1248.

(60) Röthlisberger, U.; Andreoni, W.; Giannozzi, P. *J. Chem. Phys.* **1992**, *96*, 1594.

(61) Elbayyariz, Z.; Erkoc, S. *Phys. Status Solidi B: Basic Res.* **1992**, *170*, 103.

(62) Peslherbe, G. H.; Hase, W. L. *J. Chem. Phys.* **1994**, *101*, 8535.

(63) Streitz, F. H.; Mintmire, J. W. *Phys. Rev. B* **1994**, *50*, 11996.

(64) Claire, P. d. S.; Peslherbe, G. H.; Hase, W. L. *J. Phys. Chem.* **1995**, *99*, 8147.

(65) Peslherbe, G. H.; Hase, W. L. *J. Chem. Phys.* **1996**, *104*, 9445. Claire, P. de S.; Hase, W. L. *J. Chem. Phys.* **1996**, *100*, 8190.

(66) Peslherbe, G. H.; Hase, W. L. *J. Chem. Phys.* **1996**, *105*, 7432.

(67) Peslherbe, G. H.; Hase, W. L. *J. Phys. Chem. A* **2000**, *104*, 10566.

(68) Kumar, V. *Phys. Rev. B* **1998**, *57*, 8827.

(69) Lloyd, L. D.; Johnston, R. L. *Chem. Phys.* **1998**, *236*, 107. Lloyd, L. D.; Johnston, R. L. *J. Chem. Soc., Dalton Trans.* **2000**, *3*, 307. Lloyd, L. D.; Johnston, R. L.; Roberts, C.; Mortimer-Jones, T. V. *ChemPhysChem* **2002**, *3*, 408.

(70) Ahlrichs, R.; Elliott, S. D. *Phys. Chem. Chem. Phys.* **1999**, *1*, 13.

(71) Rao, B. K.; Jena, P. *J. Chem. Phys.* **1999**, *111*, 1890.

(72) Dolgounitcheva, O.; Zakrzewski, V. G.; Ortiz, J. V. *J. Chem. Phys.* **1999**, *111*, 10762.

(73) Turner, G. W.; Johnston, R. L.; Wilson, N. T. *J. Chem. Phys.* **2000**, *112*, 4773.

(74) Geske, G. D.; Boldyrev, A. I.; Li, X.; Wang, L. S. *J. Chem. Phys.* **2000**, *113*, 5130.

(75) Zope, R. R.; Baruah, T. *Phys. Rev. B* **2001**, *64*, 053202.

(76) Deshpande, M. D.; Kanhere, D. G.; Vasiliev, I.; Martin, R. M. *Phys. Rev. B* **2003**, 035428.

(77) Joswig, J.-O.; Springborg, M. *Phys. Rev. B* **2003**, *68*, 085408.

(78) Schultz, N. E.; Staszewski, G.; Staszewski, P.; Truhlar, D. G. *J. Phys. Chem. B* **2004**, *108*, 4850.

(79) Sebetci, A.; Güvenç, Z. B. *Modeling Simul. Mater. Sci. Eng.* **2005**, *13*, 683.

(80) Peng, P.; Li, G.; Zheng, C.; Han, S.; Liu, R. *Sci. China Ser. E* **2006**, *49*, 385.

(81) Li, Z. H.; Bhatt, D.; Schultz, N. E.; Siepmann, J. I.; Truhlar, D. G. *J. Phys. Chem. C* **2007**, *111*, 16227.

(82) Liu, R. S.; Dong, K. J.; Tian, Z. A.; Liu, H. R.; Peng, P.; Yu, A. B. *J. Phys.: Condens. Matter* **2007**, *19*, 19613.

(83) Akola, J.; Manninen, M. *Phys. Rev. B* **2001**, *63*, 193410.

(84) Böyükata, M.; Güvenç, Z. B. *Brazilian J. Phys.* **2006**, *36*, 720.

(85) Puri, P.; Yang, V. *J. Phys. Chem. C* **2007**, *111*, 11776.

(86) Poland, D. *J. Chem. Phys.* **2007**, *126*, 054507.

(87) Yang, M.; Jackson, K. A.; Koehler, C.; Frauenheim, T.; Jellinek, J. *J. Chem. Phys.* **2006**, *124*, 24308.

(88) Jasper, A. W.; Staszewski, P.; Staszewski, G.; Schultz, N. E.; Truhlar, D. G. *J. Phys. Chem. B* **2004**, *108*, 8996. Jasper, A. W.; Schultz, N. E.; Truhlar, D. G. *J. Phys. Chem. B* **2005**, *109*, 3915.

(89) Bhatt, D; Jasper, A. W.; Schultz, N. E.; Siepmann, J. I.; Truhlar, D. G. *J. Am. Chem. Soc.* **2006**, *128*, 4224. Bhatt, D.; Schultz, N. E.; Jasper, A. W.; Siepmann, J. I.; Truhlar, D. G. *J. Phys. Chem. B* **2006**, *110*, 26135.

(90) Li, Z. H.; Truhlar, D. G. *J. Phys. Chem. C* **2008**, *112*, 11109.

will show that it may not be appropriate to call the structural transition or isomerization process of clusters a melting transition while nanoparticles do have a melting transition. (It is only an accident, but a convenient one, that the border between melting behavior and no-melting behavior occurs so close to the rather arbitrary border we established between nanoparticles and clusters.) The present investigations indicate that Al_n nanoparticles have a wide temperature window of coexistence of solid and liquid states; this coexistence regime is called the slush state.[9,11,92] Definitions of the solid, slush, and liquid states of such particles will be proposed.

2. Simulation Methodology

Simulations were run for Al_n with $10 \leq n \leq 300$. For $n = 10-130$, all MD simulations were started in the vicinity of the global energy minimum (GM) structures with random initial coordinates and momenta distributed according to the classical phase space distribution of separable harmonic oscillators.[64] For $n = 10-65$, GM structures obtained previously[48] have been used. For $n = 70-130$, the same strategy as used in ref 48 was used to locate GM structures. The caloric curve was then studied by heating. For larger particles, a search for the GM structure is too expensive; instead, the MD trajectory was started at high temperature with spherical clusters with atomic coordinates randomly generated in a sphere with a radius of 16, 16, and 19 Å for $n = 177, 200$, and 300, respectively, and the process simulated is the cooling process. For each heating simulation the starting temperature is 200 K with an increment of 20 K and the ending temperature is 1700 K, while for cooling simulation the same procedure is reversed.

To determine the local minima that the trajectory visited during the simulation, intermediate configurations were quenched at random; on average, 10% were quenched. Geometries of the quenched structures were optimized.

Details of solving the equations of motion, thermostatting, the heating and cooling programs, and optimization are provided in the Supporting Information.

Several properties have been investigated.

(1) Berry Parameter. The Berry parameter[93,94] is the relative root-mean-square fluctuation in the interatomic separation; it is an extension of the original Lindemann parameter[95] used for macroscopic systems. The Berry parameter is calculated by

$$\Delta_B = \frac{2}{n(n-1)} \sum_{i<j} \frac{\sqrt{\langle r_{ij}^2 \rangle - \langle r_{ij} \rangle^2}}{\langle r_{ij} \rangle} \quad (3)$$

where r_{ij} is the distance between two atoms i and j.

(2) Heat Capacity. For a macroscopic system the heat capacity at constant volume ($C \equiv dE_{Tot}/dT$, where E_{Tot} is the total energy of the system) is related to the fluctuation in energy by[96]

$$C = \frac{\langle E_{Tot}^2 \rangle - \langle E_{Tot} \rangle^2}{k_B T^2} \quad (4)$$

(See page S-3 in the Supporting Information for a discussion of the derivation.) Although the derivation of eq 4 is not directly applicable to finite systems, we found that the two sides of eq 4

agree well with each other (see Figure S-1 in the Supporting Information), and hence, we can use whichever is more convenient (we found it is more convenient to use the right-hand side). In presenting our results we convert the heat capacity to a unitless specific heat capacity c defined by

$$c = \frac{C}{(3n-3)k_B} \quad (5)$$

where the denominator results from the fact that only overall translational motion was removed in the MD simulations. In the rest of the article we will simply refer to c as the heat capacity, but we should keep in mind that the absolute heat capacity is actually C.

(3) Average Distance to the Center of Mass (R_{CoM}).[97] R_{CoM} is a property to characterize the size of a particle

$$R_{CoM} = \frac{1}{n} \sum_i |\mathbf{r}_i - \mathbf{r}_{CoM}| \quad (6)$$

where $\mathbf{r}_i$ is the vector position of an atom i and $\mathbf{r}_{CoM}$ is the vector position of the center of mass.

(4) Radius of Gyration (R_g).[98] R_g is another property that can be used to characterize the size of a particle

$$R_g = \sqrt{\frac{1}{n} \sum_i |\mathbf{r}_i - \mathbf{r}_{CoM}|^2} \quad (7)$$

(5) Volume (V). For a spherical object with evenly distributed mass, it is easy to show that the radius of the sphere has the following relationship with the principal moment of inertia (I)

$$R = \sqrt{5/2}\sqrt{I/M} \quad (8)$$

where M is total mass of the particle. Since a particle need not be spherical, we consider the three principal moments of inertia. Corresponding to these, there are three radii, R_i ($i = 1, 2, 3$). With these three radii, the volume of a particle can be estimated as[27]

$$V = \frac{4}{3}\pi R_1 R_2 R_3 \quad (9)$$

The quantity V was calculated at each step of the molecular dynamics simulation and averaged.

(6) Coefficient of Thermal Expansion (β).

$$\beta = \frac{1}{V}\frac{dV}{dT} \quad (10)$$

In the current study, the temperature derivatives of V and other properties were obtained by first fitting them with cubic spline functions and then differentiating the fitted spline functions.

(7) Isothermal Compressibility (κ).[99]

$$\kappa = \frac{1}{k_B T}\frac{\langle V^2 \rangle - \langle V \rangle^2}{\langle V \rangle} \quad (11)$$

where V is calculated by eq 11.

3. Results

3.1. Berry Parameter. Although the Berry parameter (Δ_B) has been widely used to study the melting of clusters and nanoparticles,[6,9,14,19,27,33,34,84,93,94] our simulations show that it is more sensitive to geometrical transitions than other properties

(91) Schultz, N. E.; Jasper, A. W.; Bhatt, D.; Siepmann, J. I.; Truhlar, D. G. In *Multiscale Simulation Methods for Nanomaterials*; Ross, R. B., Mohanty, S., Eds.; Wiley-VCH: Hoboken, NJ, 2008; p 169.
(92) Tanner, G. M.; Bhattacharya, A.; Nayak, S. K.; Mahanti, S. D. *Phys. Rev. E* **1997**, *55*, 322.
(93) Kaelberer, J.; Etters, R. D *J. Chem. Phys.* **1977**, *66*, 3233. Etters, R. D.; Kaelberer, J. *J. Chem. Phys.* **1977**, *66*, 5112.
(94) Berry, R. S.; Beck, T. L.; Davis, H. L.; Jellinek, J. *Adv. Chem. Phys.* **1988**, *70B*, 75. Zhou, Y.; Karplus, M.; Ball, K. D.; Berry, R. S. *J. Chem. Phys.* **2002**, *116*, 2323.
(95) Lindemann, F. A. *Phys. Z* **1910**, *11*, 609.

(96) Hill, T. L. *Statistical Mechanics: Principles and Selected Applications*; McGraw-Hill: New York, 1956; pp 100–101. Rice, O. K. *Statistical Mechanics Thermodynamics and Kinetics*; W. H. Freeman: San Francisco, 1967; pp 92–93..
(97) Ding, F.; Rosen, A.; Bolton, K. *Phys. Rev. B* **2004**, *70*, 75416.
(98) Wang, L.; Zhang, Y.; Bian, X.; Chen, Y. *Phys. Lett. A* **2003**, *310*, 197.
(99) Pathria, R. K. *Statistical Mechanics*, 2nd ed.; Elsevier: Singapore, 1996; p 454.
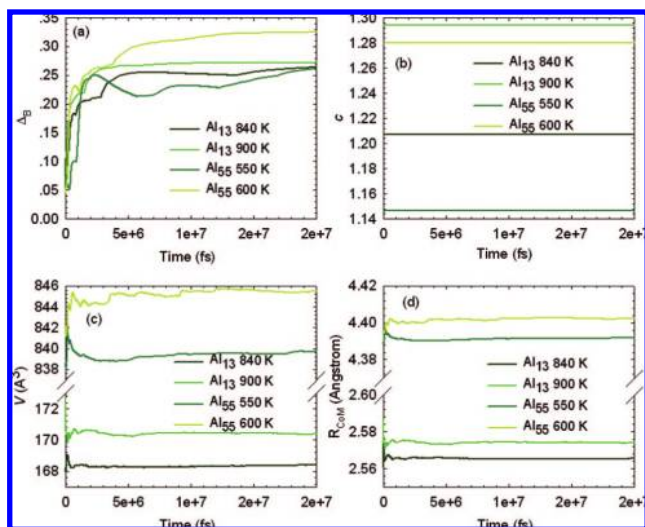
Figure 2. Convergence behavior of various properties of Al_{13} and Al_{55} in the transition region: (a) Berry parameter, (b) unitless specific heat capacity c, (c) volume, (d) average distance to the center of mass as a function of simulation time.

that may be used to characterize the system. As just one example of our findings on this subject, Figure 2a shows that the Berry parameter converges very slowly with simulation time. In fact, Δ_B obtained at 1 and 5 ns may differ by more than a factor of 2. For Al_{55} at 550 K, after 20 ns, Δ_B still shows no sign of convergence. However, other properties show much better convergence behavior (see Figure 2b–d). In Figure 3 several properties are plotted as functions of temperature for Al_{55} obtained with two different simulation times. The plots indicate that for the Berry parameter different simulation times may give very different results (Figure 3a) unless very long simulations are run. For the other properties, plots of the property vs T obtained with different simulation times almost overlap with each other. Moreover, the Berry parameter plots indicate that the most dramatic structural change occurs at about 600 and 550 K for the short time and long time simulation, respectively. On the other hand, the other plots indicate that the most dramatic changes in all the other properties of the nanoparticles occur at about 650 K. Since the diffusion constant is related to the average square displacement of an atom[100]

$$D = \lim_{t \to \infty} \frac{1}{6t} \langle |\mathbf{r}_i(t) - \mathbf{r}_i(0)|^2 \rangle \tag{12}$$

the Berry parameter is greatly affected by the diffusion of individual atoms, which occurs slowly in the transition regime. The jumps in the Δ_B plots (Figure 2a) may be due to the jump of an atom to other positions.[101] Beck et al. also noted that Δ_B can become quite large if any transitions occur between local potential minima.[9] Indeed, for some clusters where low-energy minima are in equilibrium at low temperatures,[48] Δ_B is as large as 0.2 at a temperature as low as 200 K (Figure S-14 in the Supporting Information).

Therefore, we focus on other properties and found the heat capacity, radius, and volume to be particularly useful. For practical purposes, using the multiple-simulation, multiple-equilibration protocol explained in the Supporting Information,

we found that consistent results can be obtained with these other properties even in runs in which the Berry parameter is not yet converged in individual simulations, and we shall use these other properties in the rest of the paper. The general success of this approach may result from high-energy states contributing less to other properties than to the Berry parameter, an interpretation which is consistent with (but not proved by) our simulation results. The result has general implications for simulations in that often one can achieve a similar understanding of a system from one or another observable, but one of these observables may converge more quickly than the other.

3.2. Heat Capacity. Three typical kinds of c curves are plotted in Figure 4. Curves for all other particles are available in the Supporting Information.

The first type of c curve has a well-defined peak such that c increases almost linearly with temperature before the peak and after the peak c decreases almost linearly with temperature. Careful examination of the plots shows that Al_{51}, Al_{70}, Al_{80}, Al_{90}, Al_{100}, Al_{110}, Al_{120}, Al_{130}, Al_{177}, Al_{200}, and Al_{300} exhibit a quasiplateau in the peak region. For this type of curve, the peak (plateau) becomes narrower and higher as the particle size increases, which demonstrates a trend toward bulk behavior. Plots for Al_{120}, Al_{130}, Al_{177}, Al_{200}, and Al_{300} (see Supporting Information) are all similar to that for Al_{130}. The trend toward bulk behavior has been examined before in model systems,[102] and the present results are consistent with this previous work. All plots for the 11 particles listed above show a bump at about 900 K, probably indicating a state change.

The second type of c curve, shown in Figure 4b, features a big bump in the curve rather than a peak. For this type, c increases gradually before the bump, where it reaches a maximum value and then decreases almost linearly at high temperatures. The bump does not become narrower as particle size increases. The third type of caloric curve, shown in Figure 4c, can be viewed as a superimposition of one or more small peaks before the maximum of the second type of curve.

For particles with $n \leq 18$, the maximum of the peak in c is either so high that the decrease at high temperatures is a part of the peak tail or so low (for Al_{10}, Al_{11}, and Al_{18}) that the curve goes flat at high temperatures. Putting c plots (Figure 4d) of Al_{10}–Al_{18} (left) and those of Al_{19}–Al_{300} (right) on two separate graphs shows that they can be classified into two different groups; for the second group, heat capacities of most particles decrease almost linearly with temperature after 900 K.

The temperature T_p at which c has a maximum is determined as the zero of dc/dT ($= dC/dT$), where dc/dT is calculated from spline fits. For those curves with multiple peaks, we choose the one most likely corresponding to a melting transition. For example, for Al_{26}, Al_{27}, Al_{38}, Al_{43}, and Al_{58}, shown in Figure 4c, the higher peak temperature is adopted. We find that T_p does show a strong dependence on particle size (Table 1 and Figure 5). For many small particles T_p is higher than the bulk melting temperature[103] of 933 K (dashed line in Figure 5). In agreement with the experimental findings for Al_n^+ cations,[36,42–44] we find that a change of particle size by just one single atom can make a very large difference in T_p.

We are cautious about quantitatively comparing our results with experiment because the experiments are for Al_n^+ cations while our analytical potential and simulation are for neutral

(100) Einstein, A. *Investigations on the Theory of the Brownian Movement*; Methuen: London, 1926; p 17. Allen, M. P.; Tildesley, D. J. *Computer Simulation of Liquids*; Oxford University Press: Oxford, 1987; p 60.
(101) Vollmayr-Lee, K. *J. Chem. Phys.* **2004**, *121*, 4781.

(102) Wales, D. J.; Doye, J. P. K. *J. Chem. Phys.* **1995**, *103*, 3061.
(103) Chase, M. W., Jr. NIST-JANAF Thermochemical Tables, 4th ed. *J. Phys. Chem. Ref. Data*, Monograph 9; American Institute of Physics: New York, 1998.
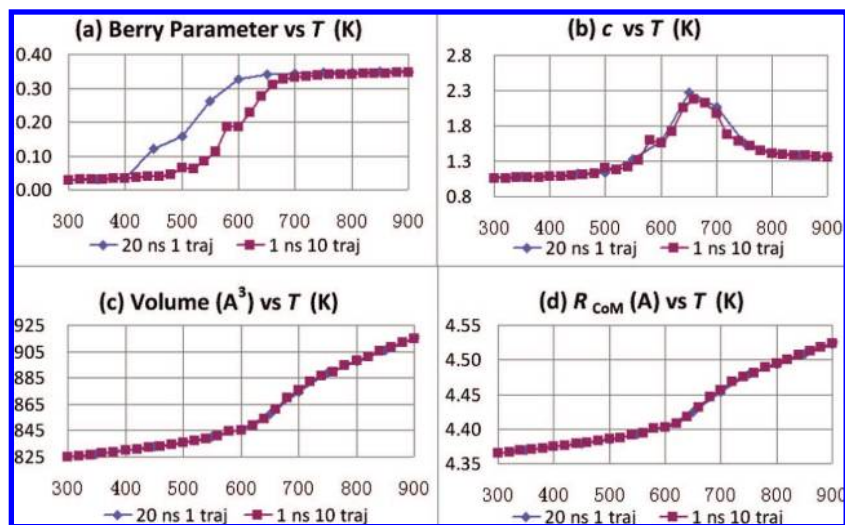
Figure 3. Convergence behavior of various properties of Al_{55}: (a) Berry parameter, (b) unitless specific heat capacity c, (c) volume, (d) average distance to the center of mass as a function of temperature. In parts c and d the results for the two lengths of simulation agree so well that one set of results is hidden behind the other.
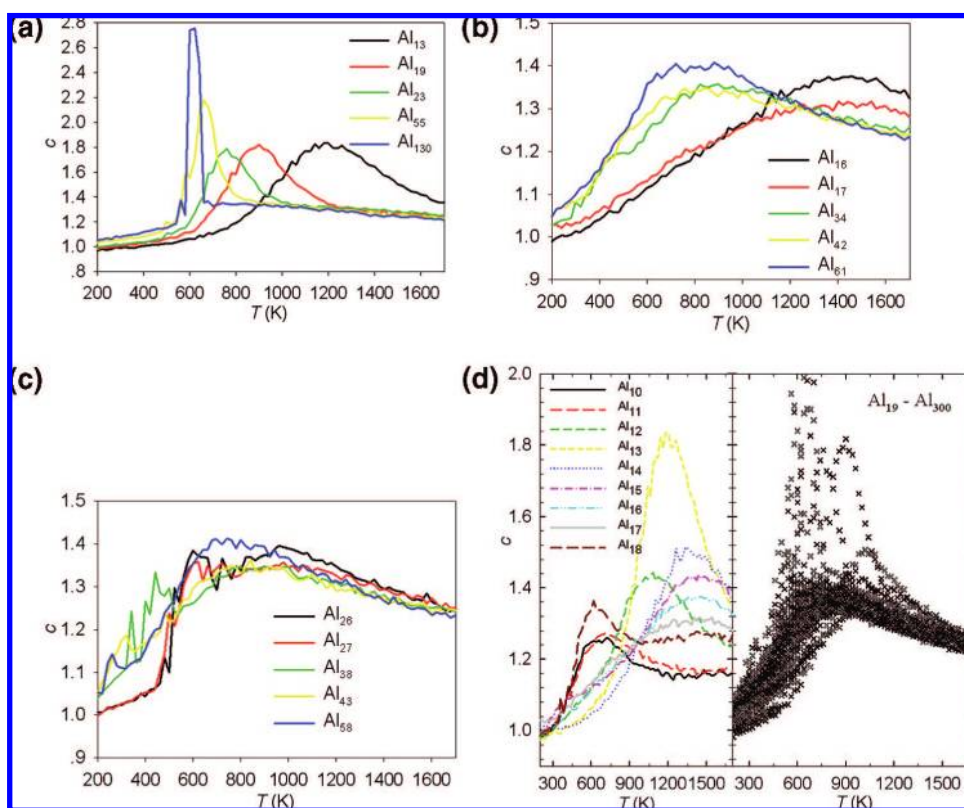

Figure 4. Unitless specific heat capacity c curves: (a) one sharp peak, (b) no sharp peak before reaching the linear region at high temperatures, (c) spikes before reaching the linear region at high temperatures, (d) for all particles, left (Al_{10}–Al_{18}) and right (Al_{19}–Al_{300}).

particles. All simulations[34,39,84] with analytical potentials including the current work failed to predict the more than 100 K drop of T_p from Al_{55} to Al_{56}.[36] If jellium or electronic closed-shell models can be applied to aluminum clusters, which is still a debatable issue,[49,50,55,68,71,76] cationic and neutral Al_n particles with the same size can be very different in physical and chemical properties, although such differences should typically become smaller as particle size increases.[55] Another reason for caution is that electronic excitation contributions to the heat capacity have been omitted in the present simulations since the potential is optimized for the ground electronic states of the particles.

The electronic excitation contribution to the heat capacity can be estimated using the electronic energy levels for the global minimum structures calculated in a previous study.[81] In the Supporting Information, we presented results for electronic contributions for several particles; electronic contributions are not negligible and thus may change the position and shape of the peak.

3.3. Average Distance to the Center of Mass, Radius of Gyration, and Volume. Since the solid state is generally more compact than the liquid state, the transition from the solid state to the liquid state may lead to significant changes in particle

Table 1. Freezing Temperature (T_f), Melting Temperature (T_m), Position of Sharp Peaks/Deep Valleys (T_p) in Unitless Specific Heat Capacity (c), Coefficient of Thermal Expansion (β), Natural Logarithm of Compressibility (ln κ), and Temperature (T_{P50}) at Which $P(0) = 50^a$

		$T_p{}^b$				
n	T_f	c	β	ln $\kappa{}^c$	T_{P50}	T_m
10	300	717	NA	NA	826	1240
11	320	708	NA	548	907	1300
12	560	1071	1225	840	NA	NA
13	700	1188	1273	1026	NA	NA
14*	NA	(347), 1353	NA	1187	NA	1480
15*	NA	1394	NA	1186	NA	NA
16*	NA	1446	NA	220	1349	NA
17*	NA	1438	NA	260	946	NA
18*	260	624	(311), (384), (456)	NA	687	1580
19	600	894	937	826	1062	1420
20*	240	471, 1025	NA	946	542	1360
21	740	1127	NA	NA	1280	1180
22*	280	1119	326	317	380	1220
23	480	759	766	679	785	1100
24	520	819	NA	755	905	1100
25*	260	936	(427), 543	510, 851	543	1000
26	420	613, 978	570	519, 676	569	960
27	420	617, 711, 971	(464)	492	544	1060
28	400	750	NA	452	600	940
29	340	868	432	431	429	860
30	340	943	(416), (623)	430	445	940
31*	NA	922	(382)	365	326	1040
32*	NA	806	240, (355)	599	429	800
33*	NA	864	NA	696	269	940
34*	260	878	346	507	364	960
35*	240	854	(305)	475	368	960
36*	NA	829	325	NA	387	940
37*	NA	834	248	320	270	940
38*	280	340, 460, 797	415	395	429	920
39*	280	743	377	368	390	920
40*	NA	796	NA	405	367	860
41*	280	821	346	335	327	840
42	NA	824	284	434	261	840
43*	240	317, 833	(265)	302	322	840
44	300	835	NA	344	363	860
45*	NA	789	NA	NA	323	860
46*	NA	615	(406)	564	323	760
47*	NA	742	NA	486	407	800
48	340	510	541	462	503	920
49	320	580	507	435	389	740
50	380	723	460	447	470	820
51	360	547	517	540	506	820
52	460	597	599	600	582	820
53	440	643	654	660	644	920
54	460	666	674	700	668	920
55	480	667	678	680	645	960
56	480	663	676	680	664	1060
57*	240	608	NA	540	307	1130
58*	NA	276, 721	300	305, 648	230	1160
59	300	773	(382)	686	429	1030
60	300	732	360	345	402	1020
61	400	730, 889	(474)	454	481	1060
62	300	823	(363)	310	388	1060
63	300	842	(335)	360	345	1040
64*	240	311, 804	(318)	320	NA	1000
65*	240	352, 868	(343)	400	360	1000
70*	NA	420, 480, 565	460	458	443	940
80*	NA	532	(299), (446)	484	NA	900
90*	240	340, 561	(365), 551	(380), 524	388	940
100*	240	340, 571	(327), 575	(360), 539	d	920
110	340	572	566	580	501	900
120	500	594	696	568	560	900
130	460	619	632	592	604	900
177	400	652	660	640	d	900
200	300	657	662	660	d	900
300	580	709	717	700	d	880

^{a} Temperatures are in Kelvin, and particles in slush state at room temperature are marked with an asterisk. ^{b} T_p is the temperature at which the given quantity has a maximum or a minimum (in parentheses). ^{c} For those ln κ without sharp peaks, T_p determined is the peak/valley position of d ln κ/dT. ^{d} Intermediate configurations were not quenched.
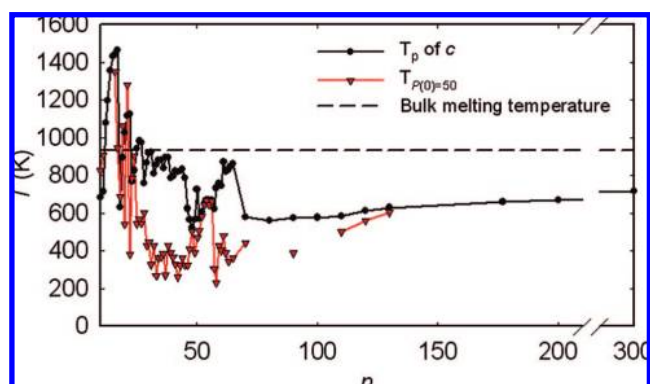
Figure 5. Peak position (T_p) of heat capacity and temperature at which $P(0) = 50$ ($T_{P(0)=50}$) as a function of cluster size. The long dashed line is the bulk melting temperature.
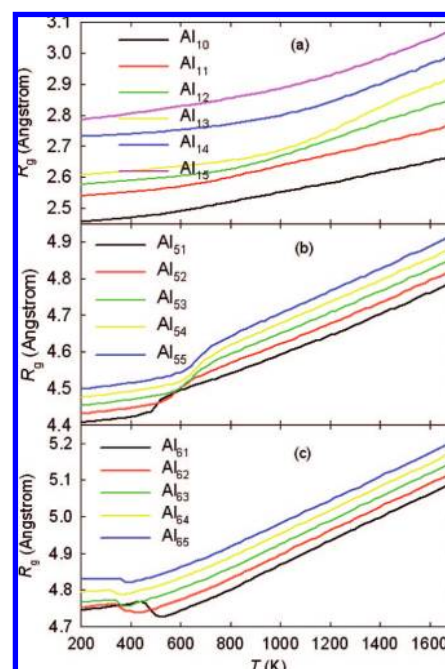

Figure 6. Three typical radius of gyration (R_g) curves: (a) change gradually with temperature, (b) obvious jumps, (c) obvious drops.

radius. We find that R_g is slightly larger than R_{CoM}, and both show similar trends with temperature; here we will focus on R_g. Figure 6 shows three typical plots of R_g vs T (the rest are in the Supporting Information). The majority of the particles studied in the present work have the first type of R_g curve, shown in Figure 6a, where R_g increases gradually with temperature. For some particles, for example, Al_{13} and Al_{19}, the curve shows a semilocalized change of slope, whereas it is almost featureless for other particles. The second type of R_g curve, shown in Figure 6b, exhibits a clear jump; this is common for large particles, especially for those particles with a well-defined sharp peak in heat capacity ($Al_{51}-Al_{56}$ and $Al_{70}-Al_{300}$). For the third type, shown in Figure 6c, R_g drops suddenly at a certain temperature and then increases gradually with temperature (Al_{27}, Al_{30}, Al_{35}, Al_{58}, Al_{59}, $Al_{61}-Al_{65}$).

Liquid nanodroplets generally have larger volumes and larger coefficients of thermal expansion (β) than solid particles with the same number of atoms. The volume has a similar dependence on temperature as R_g, and all the plots are presented in the Supporting Information. However, it is worth noting that
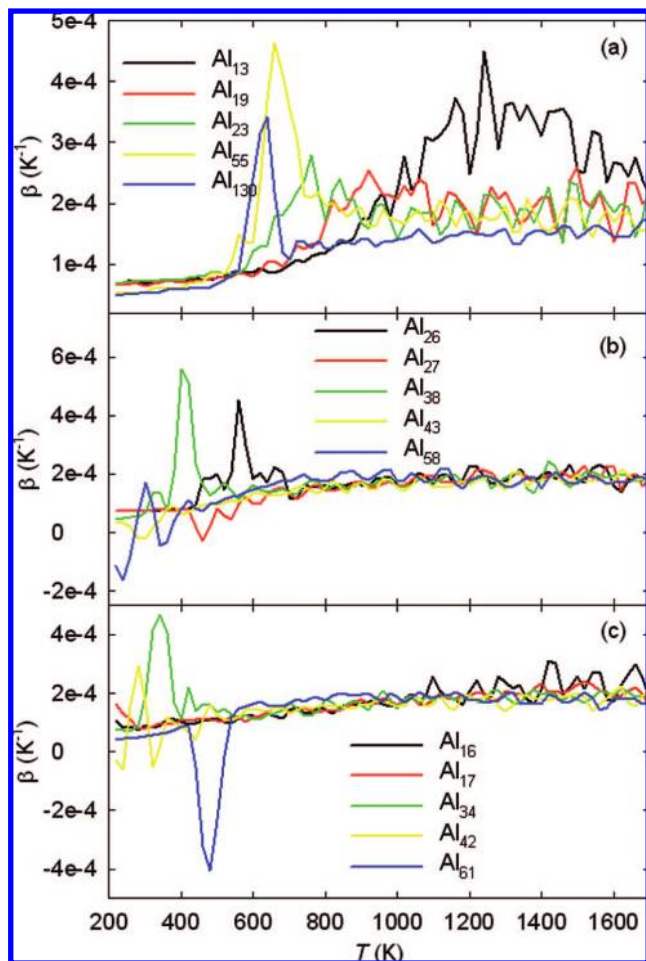
Figure 7. Coefficient of thermal expansion (β) curves: (a–c) particles with three typical heat capacity curves plotted in Figure 4.

for some particles it seems that the most stable structure at low temperatures, i.e., the solid-like structure, is not the most compact structure, the volume or R_g of the particle has a sudden drop, and the coefficient of thermal expansion has a deep valley (see below) at temperatures where the solid-like structure no longer dominates.

3.4. Coefficient of Thermal Expansion. For particles with a well-defined sharp peak in heat capacity, the coefficient of thermal expansion β also shows a well-defined sharp peak, as in Figure 7a. The positions of the peaks of β for these particles are almost the same as T_p obtained from c. For those particles having almost featureless c curves, however, the β plots give valuable new information, as illustrated in Figure 7b. For example, β of Al_{34} has a sharp peak at about 340 K, and that of Al_{61} has a deep valley at about 480 K. For most particles, if one ignores such peaks and valleys, one finds that β generally increases with temperature and then reaches a plateau at high temperatures. A clear change of slope is observed for most particles; after the change of slope, β increases more slowly with temperature and the curve shows periodic oscillations. Representative examples are provided by the particles with sizes between Al_{61} and Al_{65} (Figure 7c). Putting all these curves into one graph shows that for most particles the change of slope is at about 900 K (Figure S-8 in the Supporting Information). This indicates that after 900 K most particles are in a similar state, the liquid droplet state.
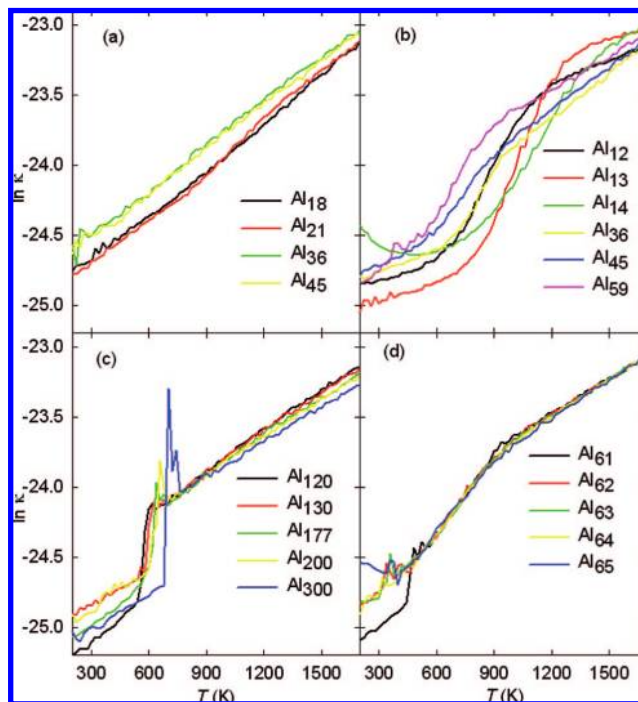

Figure 8. Typical natural logarithm of isothermal compressibility (ln κ) curves: (a) almost linear in the whole temperature range, (b) with obvious jumps, (c) with sharp peaks, (d) with two almost linear segments joined at about 1000 K.

3.5. Isothermal Compressibility. Isothermal compressibility (κ) is a function of pressure. The compressibilities calculated in the present study are the low-pressure limits because it is the free Al_n particles that are studied. Compressibilities as a function of temperature for each particle size are presented in the Supporting Information. Here we focus on the natural logarithm of compressibility. For Al_{18}, Al_{21}, Al_{36}, and Al_{45}, the ln κ vs T curve is almost linear in the whole simulation temperature range (Figure 8a). For some particles, the curve is smooth but has large curvature (Figure 8b). For most large particles the curve has a clear jump or sharp peak at a certain temperature (Figure 8c). For the particles shown in Figure 8c, before and after the jump or peak, ln κ is an almost linear function of temperature. The position of the jump or peak almost overlaps with the peak position of heat capacity. For some particles, for example, Al_{61}–Al_{65} as shown in Figure 8d, the curve has sharp changes at temperatures between 300 and 600 K. After 600 K, the curve is almost linear until about 1000 K, then the slope changes, and the curve is again linear. For Al_{62}–Al_{64}, the position of the peak between 300 and 600 K is in agreement with the small peak in the c curve (see Supporting Information), while for Al_{61}, there is no clear peak in the c curve at this temperature range. Clearly, for the particles shown in Figure 8c and 8d, there is a change of state at the point of sharp change. Putting all of the plots into one graph, an almost linear dependence of ln κ on T, similar to the functional dependences of c and β, can also be seen for most particles above 900–1000 K, but the trend is less clear than for c and β, and the plots are available in the Supporting Information.

3.6. Potential-Energy Distribution of the Quenched Structures. By quenching intermediate configurations we determined what fraction of the time is spent by trajectories in the configuration space around each local minimum (this time is proportional to the number of quenched structures corre-

sponding to that minimum). As particle size increases and the number of isomers the trajectory can visit grows exponentially, the energy distribution of the isomers becomes quasicontinuous; therefore, it is convenient to discuss these results using an energy scale rather than the ordinal numbers of the isomers. To accomplish this we counted the number of quenched structures in each specific energy range. The percentage $P(E)$ is defined as $100 \ M(E)/N_q$, where $M(E)$ is the number of quenched structures with potential energy between E and $E + \delta E$ and N_q is the total number of quenched configurations at a specific temperature. The energy resolution δE in the current study is 0.05 eV, and the zero of the energy is the energy of the global minimum, GM.

The $P(E)$ plots of some particles can be found in the Supporting Information. We found $P(0)$, the percentage of the quenched structures with an energy not higher than that of GM (including GM) by 0.05 eV, is particularly useful (see Supporting Information for the plots and also the next section). Although use of a 0.05 eV resolution for δE is somewhat arbitrary, the structures with energies not higher than GM by 0.05 eV can be viewed as structures almost degenerate in energy with GM. Since these low-energy isomers (including GM) are the dominant structures at low temperatures and often have compact and well-ordered structures,[48] they probably can be viewed as solid-like structures, while other higher-energy isomers can often be viewed as liquid-like structures. (One must bear in mind that there will hardly be a clear border between solid-like and liquid-like structures.[11]) Therefore, the equilibrium constant between the solid state and liquid state is related to $P(0)$ by

$$K_{eq} = \frac{100 - P(0)}{P(0)} \qquad (13)$$

If we define the temperature at which $K_{eq} = 1$ ($P(0) = 50$) as the population-based melting temperature (T_{P50}), another quantity characterizing the melting transition of clusters and nanoparticles can be defined; such values are given in Table 1. However, for some small particles (for example, Al_{13}) $P(0)$ is never under 50, while for some particles (for example, Al_{80}) $P(0)$ never exceeds 50 in the simulation temperature range we studied. Therefore, for these particles a population-based melting temperature defined this way cannot be obtained. The T_{P50} values are compared to T_p values in Figure 5. It can be seen that for those particles with well-defined sharp peaks in heat capacity T_p of heat capacity and T_{P50} generally agree well with each other, while for other particles T_{P50} generally agrees better with the T_p of β or $\ln \kappa$ (Table 1).

We also analyzed the potential-energy distribution ($\rho(E)$) of the distinct isomers in the quenched structures. $\rho(E)$ is defined as $dn(E)/dE$, where $dn(E)$ is the number of distinct isomers in the energy range E to $E + dE$. The distribution is obtained by a Legendre moment method[104] with the l of the normalized Legendre polynomial $P_l(x)$ truncated at $l_{max} = 30$ for $Al_{10}-Al_{15}$ and $l_{max} = 40$ for the rest. In Figure 9 we plotted the potential-energy distribution ($\rho(E)$) of distinct isomers for $Al_{10}-Al_{27}$.

4. Discussion

4.1. Magic Structures and First-Order Melting Transitions. Al_{13} is the most extensively studied of the clusters.[14,61,72,75,80,83,85] We find that Al_{13} has a very large energy gap (1.01 eV) between the GM and the second lowest energy
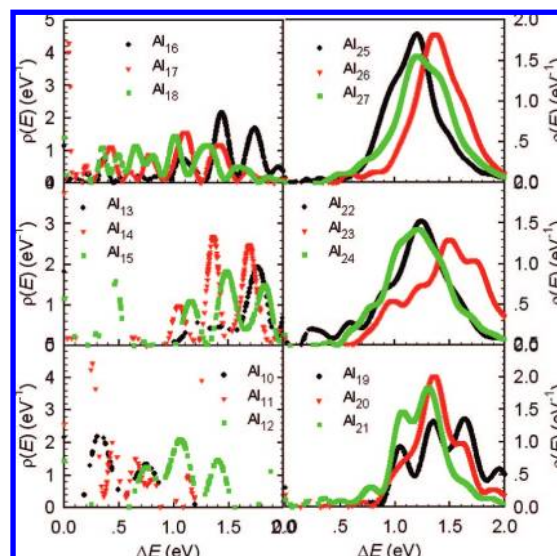

Figure 9. Potential-energy distribution ($\rho(E)$) of the nonidentical structures quenched in the MD simulations. The abscissa is the relative potential energy to the global minimum structure.
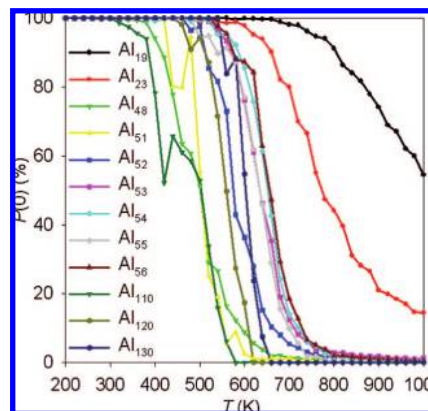

Figure 10. $P(0)$ (see text for definition) for particles with a single sharp peak in c and β and single sharp peak or obvious jump in $\ln \kappa$.

isomer, and ab initio calculations indicate that there is a very high energy barrier between the two lowest energy structures.[80] Therefore, Al_{13} has extraordinary structural stability. It may therefore be called a magic structure or, since it also keeps its structure in chemical reactions, a superatom.[105] Our results indicate that the icosahedral structure of Al_{13} is dominant as high as 1700 K. As in most studies, we find that the peak of c occurs at a very high temperature.

Among the larger particles, Al_{19}, Al_{23}, Al_{48}, $Al_{51}-Al_{56}$, and $Al_{110}-Al_{300}$ are particles that have a single well-defined peak in c and β, respectively, a clear jump or sharp peak in $\ln \kappa$, a jump in R_g, and, except for Al_{19}, a jump in V; Al_{19} has a clear transition point in R_g and V. Analogously to macroscopic systems, the melting transition for these particles can be called a first-order phase transition[42–44] or single-phase transition.[33] A common feature of these particles is that the low-energy isomers between 0 and 0.05 eV are dominant up to about 500 K. In Figure 10 we plotted $P(0)$ for Al_{19}, Al_{23}, Al_{48}, $Al_{51}-Al_{56}$, and $Al_{110}-Al_{130}$ as a function of temperature. For these particles,

(104) Truhlar, D. G.; Blais, N. C. *J. Chem. Phys.* **1977**, *67*, 1532.

(105) Bergeron, D. E., Jr.; Morisato, T.; Khanna, S. N. *Science* **2004**, *304*, 84. Bergeron, D. E., Jr.; Morisato, T.; Khanna, S. N. *J. Chem. Phys.* **2004**, *121*, 10456.

$P(0)$ is still higher than 50 at 500 K. In the cases of Al_{19}, Al_{23}, Al_{48}, Al_{54}, Al_{55}, and Al_{120}, there is a large energy gap between the GM and the second lowest energy isomer; we find gaps of 0.66, 0.55, 0.20, 0.70, 0.70, and 0.30 eV, respectively. For the other particle sizes, there are several or many low-energy isomers that are almost degenerate in energy with the GM and separated from higher-energy structures by a large energy gap; these low-energy isomers also have similar structure and probably can be viewed as solid-like structures just like the GM structure. (Recall that a finite-temperature macroscopic solid state is not a single quantum state but rather a large number of quantum states with similar energy and properties; this behavior is seen here at the threshold of emergence.) Al_{56} is a prototype of such particles.[48] For Al_{56}, the GM and second and third lowest-energy structures can be viewed as attaching an aluminum atom to the icosahedron Al_{55}. There are also 52 other isomers, all with similar geometry, with energy just higher than the GM by less than 0.07 eV. The rest are higher in energy by 0.41 eV. Our previous study indicates that the properties of the Al_{56} particle can be well represented by the GM in a wide temperature range.[48] Therefore, for those particles with a first-order melting transition there is a large energy gap between, on the one hand, the GM or the solid-like structures and, on the other hand, the liquid-like structures.

Although an energy gap between isomers is one important determinant of the distribution of isomers, the distribution function depends on *free* energy, which also has an entropic component, and the entropic contribution determined by the density of vibrational and rotational states in each isomer is also important.[48] As an apparent consequence, the existence of a large energy gap is not in one-to-one correspondence with the existence of a single sharp peak in the heat capacity. Al_{38} and Al_{61} are prototypes for the dominance of the entropic effect. The energy gaps between the two lowest-energy isomers are large, 0.45 and 0.25 eV, respectively. However, Al_{38} has two small peaks in c before c reaches a maximum, while there is no well-defined peak in c for Al_{61} (see Table 1 and the Supporting Information). Some studies also found a small peak in c for Al_{38} and attribute this peak to a premelting process.[33] Since the GMs of Al_{38} and Al_{61} are closely packed and well-ordered structures,[48] it seems that the geometrical order in the electronic ground-state GM structure is not an adequate but just a necessary condition for a magic melter, in contrast to the findings in gallium particles.[32,38] The entropy effect must be taken into consideration.[44−49]

Finally, we consider the Gibbs−Thomson relation[23,106] and other similar relations such as the Pawlow relation,[107,108] which establish a linear relationship between the melting temperature of a particle and the reciprocal of the particle radius ($1/R$). In Figure 11 the temperature T_p at which the heat capacity has a maximum is plotted as a function of $1/R$, where R is estimated as[109] $R = \sqrt{5/3}R_g$. Since R_g is a function of temperature, we use R_g values obtained from two temperatures, 200 and 1500 K, to make the plots. Figure 11 shows that the choice of R_g does not affect the qualitative correlation or lack of correlation between T_p and $1/R$ much, and it shows that only for particles with size $n > 70$ does T_p depend linearly on $1/R$, whereas for small particles there is no such relationship. One possible cause
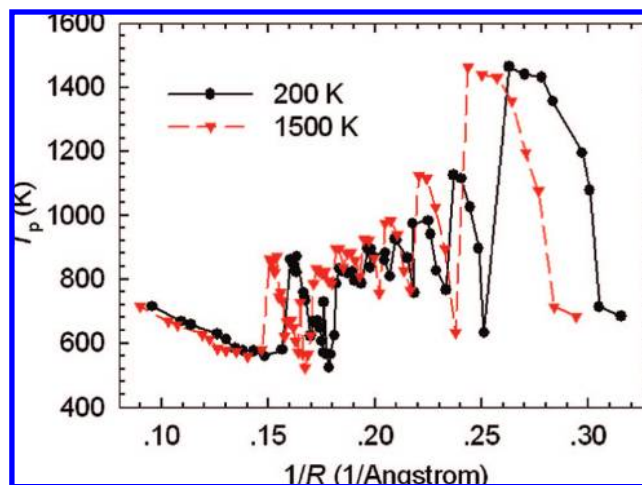
(106) Thomson, W. *Philos. Mag.* **1871**, *42*, 448.
(107) Pawlow, P. Z. *Phys. Chem.* **1909**, *65*, 1.
(108) Borel, J. P. *Surf. Sci.* **1981**, *106*, 1.
(109) Wang, L.; Zhang, Y.; Bian, X.; Chen, Y. *Phys. Lett. A* **2003**, *310*, 197.

Figure 11. Plots of the temperature T_p at which c has a maximum as a function of $1/R$, where R is the particle radius estimated from the radius of gyration (R_g) by $R = \sqrt{5/3}R_g$. R_g values obtained at 200 (straight line) and 1500 K (dashed line) are used to make the plots.

of the deviation from the linear relationship is that for small particles T_p is not a very good quantity to characterize the melting of a particle (see below). Another possible contributor may be that small aluminum particles are not spherical (aluminum nanodroplets are prolate[91]), which is a precondition in deriving such relations. The present results confirm that macroscopic models such as the Pawlow relation do not explain the interesting properties of finite systems.

4.2. Clusters (<1 nm, $n \leq 18$) Have No Melting Transition. In the Results section, we presented various physical properties of Al_n particles that are supposed to change if a particle changes from the solid state to the liquid state. We find startlingly different behavior for different size particles. The simulations provide a much more detailed picture of the phase characteristics than is available experimentally. In particular, as assortment of properties may be monitored. One may use these properties to characterize the melting of clusters and nanoparticles; however, phase transitions in finite systems are more complicated than those in macroscopic systems since phase is not well defined in finite systems. For example, as shown in the Introduction, a peak in the heat capacity curve does not necessarily correspond to a melting transition; it may just result from the equilibrium between isomers, such as in the cases of the clusters Al_{10}, Al_{11}, Al_{12}, and Al_{13}. For each of these four clusters we observe a well-defined peak in the heat capacity curve.

The $P(E)$ plots for Al_{11} and Al_{13} are presented in Figure 12, and the plots for Al_{10} and Al_{12} (given in the Supporting Information) are similar to those for Al_{11} and Al_{13}, respectively. For these four clusters the energy gap between the GM and the second lowest energy isomer is larger than 0.05 eV, and thus, $P(0)$ is the percentage population of the GM structure. For Al_{11}, the temperature T_p of the peak in c is 708 K (Table 1). At this temperature, GM structures still have about 70% population (see Figure 12a). Between 700 and 900 K, isomers between 0.15 and 0.25 eV are the next most abundant and the plot shows a peak at 0.20 eV. After 900 K, the peak shifts to 0.30 eV. There are a total of 74 nonidentical isomers in the energy range between 0.15 and 0.45 eV. After 708 K, the Al_{11} particle is a mixture of the GM, the 74 isomers between 0.15 and 0.45 eV,
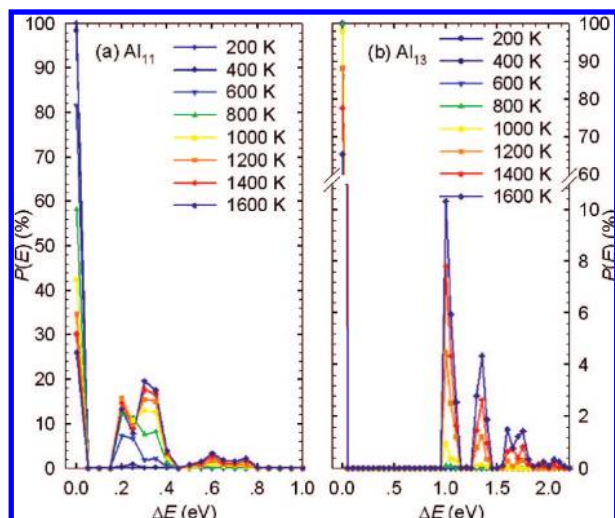
Figure 12. Percentage ($P(E)$) of quenched structures in the potential-energy range between E to $E + \delta E$ with $\delta E = 0.05$ eV: (a) Al_{11} and (b) Al_{13}. The abscissa is the relative potential energy to the global minimum structure.
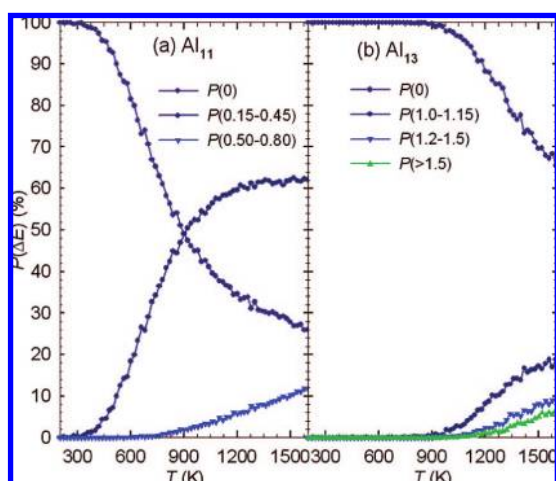

Figure 13. Percentage ($P(E)$) of quenched structures in the three potential-energy ranges corresponding to the three (Al_{11}) or four (Al_{13}) different regions as shown in Figure 9: (a) Al_{11} and (b) Al_{13}. $P(0)$ is the percentage population of the global minimum structures.

and the 48 isomers between 0.50 and 0.80 eV (Figure 13a). At 1600 K, 25% of the quenched structures are still the GM structure.

For Al_{13}, the peak of c is at 1188 K and the GM structure still constitutes about 90% of the quenched structures at this temperature. At 1600 K, more than 65% the quenched structures are the GM structure. Thus, in the whole simulation temperature range, Al_{13} is usually in the region of coordinate space around the most stable structure, which is a very well-ordered isosahedral structure. If we call this structure the solid-like structure and the other less stable isomers (about 150 of them between 1.0 and 2.0 eV) the liquid-like structures, we can summarize this situation by saying that Al_{13} never fully melts in the temperature range we studied and neither does Al_{10}, Al_{11}, or Al_{12} (see also Supporting Information).

From another point of view, some of the properties of small clusters can be understood by analogy to conventional molecules. Usually, when studying molecules, the change from one isomer to another isomer with a distinct structural difference is called an isomerization reaction. For small clusters, the number

of local-minimum structures (isomers) that the trajectory can visit in the simulation temperature range is limited. For example, only 64, 138, 167, 217, 228, 387, 907, 832, 1266, 1725, and 2354 nonidentical isomers have been found for Al_{10}–Al_{20} clusters. The number of isomers the trajectory most often visits is even smaller. For example, for Al_{16} and Al_{17} more than 90% of the time the trajectory visits only 8% (74 out of 907) and 30% (247 out of 832) of the low-energy isomers, respectively. Therefore, even at high temperatures, these clusters are a mixture of a limited number of isomers.

The potential-energy distribution ($\rho(E)$) of the distinct isomers also indicates that clusters behave more like molecules than nanoparticles do. From the $\rho(E)$ plots (Figure 9) it is clear that for particles smaller than Al_{19} the energy distribution of isomers is scattered (Al_{10}–Al_{15}) or has well-separated multiple peaks with comparable heights (Al_{16}–Al_{18}). Only for Al_n particles with $n \geq 19$ does the distribution for high-energy isomers have a roughly Gaussian distribution, and these isomers can be viewed as being in one state, the liquid state.

We can conclude that clusters have no melting transition, or in other words, they are too small to melt.[31] The measured or simulated caloric curves of these clusters are better understood as resulting from molecule-like isomerization processes than from macroscopic-like melting transitions.

4.3. Solid, Slush, and Liquid States in Clusters and Nanoparticles. The discussion above raises a basic question: What are the solid and liquid states for clusters and nanoparticles? Or even more basically, what is phase for clusters and nanoparticles?[9] Due to the enormous number of atoms in a macroscopic system, the change from one phase to another phase is accompanied by a noncontinuous change in certain physical or chemical properties.[9,11,20,21] The discontinuity is called a first-order phase transition (ϕ) and characterized by a temperature T_ϕ. At T_ϕ, the two phases are in equilibrium and $K_{eq} = 1$. Thus, once these T_ϕ points have been determined as functions of pressure or volume, the regimes of the phases are known. However, for finite systems, especially clusters and small nanoparticles, one has to abandon the concept of a precise T_ϕ and recognize the fact that different "phases", if there are any, of clusters and nanoparticles are in equilibrium with each other in an appreciable temperature range.[9,11,15–18,25,37,41] The results for small clusters such as Al_{11}–Al_{13} that are discussed above indicate the problematic character of using solely the caloric curves to characterize the melting transition.

As particle size increases, the solid and liquid states of nanoparticles can be defined with less ambiguity. We start our discussion with the most macroscopic-like particle, Al_{300}. For this particle, all properties give consistent results, implying that there is a state change at about 700 K (Figure 14): (i) c has a very high and sharp peak at about 700 K (Figure 14a). Before 600 K, c increases almost linearly with temperature. Between 760 and 880 K, c reaches a plateau (see also Figure S-3n in the Supporting Information) and then decreases almost linearly with temperature. (ii) R_g and V jump between 680 and 760 K (Figure 14b); aside from this region, they are both smooth functions of temperature. (iii) β increases almost linearly with temperature below 580 K (Figure 14c); after 560 K, the plot shows a small peak at 600 K, a valley at 640 K, and a high peak at 720 K. After the high peak, β drops and reaches a valley at 780 K. After 820 K, the plot shows an oscillatory behavior; averaging out these oscillations yields a β that increases almost linearly with temperature. (iv) The logarithm of κ (ln κ) increases almost linearly with temperature below 680 K (Figure 14d). Then it
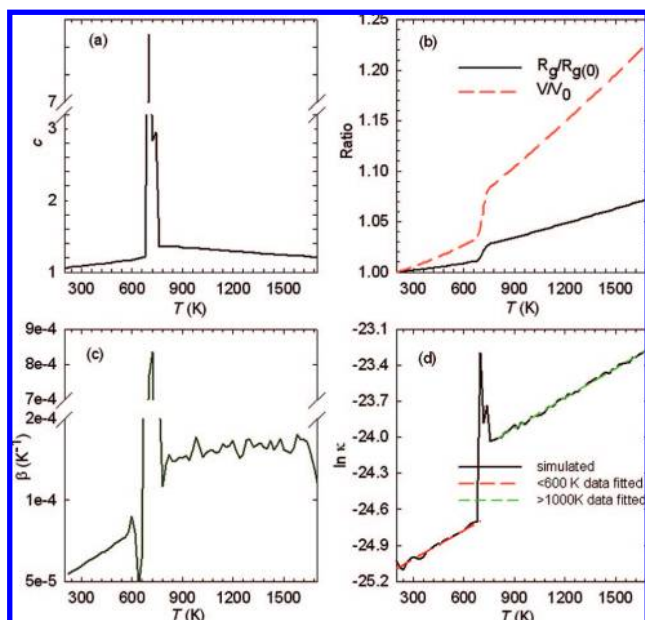
Figure 14. Four properties used to characterize the melting transition of Al_{300}: (a) heat capacity, (b) $R_g/R_{g(0)}$ and V/V_0 where $R_{g(0)}$ and V_0 are the radius of gyration and volume, respectively, at 200 K, (c) coefficient of thermal expansion, (d) natural logarithm of isothermal compressibility. The sudden drop after 1600 K in b may be due to the abnormalities in the spline fitting functions to obtain dV/dT (see also Figure S-1) since volume is very smooth after 1600 K. The long dashed and short dashed lines in d are least-squares fits to data points below 600 K and above 1000 K, respectively; the line at high temperatures has a slightly steeper slope than the one at low temperatures.

reaches a high peak at 700 K and a low peak (a shoulder in the plot) at 740 K. After 760 K, it again increases almost linearly with temperature.

Note that an equilibrium mixture of coexisting isomers in a nanoparticle is qualitatively different from the equilibrium between separated phases in a macroscopic system. Nevertheless, based on the phase definition used for macroscopic systems,[20,21] it is clear that for Al_{300} there are two distinctly different states, one at low temperatures below 580 K and one at high temperatures above 880 K. At low temperatures the particle has a smaller radius, volume, coefficient of thermal expansion, and compressibility than does the particle at high temperatures. Thus, the particle is in the solid state in the low-temperature range and in the liquid state in the high-temperature range. In these two states, c, β, and $\ln \kappa$ are almost linear functions of temperature after averaging out the weak periodic oscillations. The coexistence region is between 580 and 880 K. Detailed analysis of these three properties indicates that, from one point of view, there is more than one "state" in this region (for example, see Figure 14d),[36,44] but the temperature window for each "state" can hardly be singled out by analyzing the three physical properties. Following the convention of Beck, Jellinek, and Berry,[9] we shall call this situation a slush state.

In the previous paragraph, we roughly determined the freezing temperature T_f and melting temperature T_m for Al_{300}. The same analysis was applied to other large particles. For example, for Al_{200}, T_m can be roughly determined as 900 K. We also find that T_f of Al_{200} may be as low as 300 K because c, β, and $\ln \kappa$ plots all show a rough region around 400 K, indicating some sort of structural transition in this region. For Al_{177}, T_f is about 400 K and T_m is about 900 K. For Al_{55}, T_f is about 480 K and T_m is about 960 K.

Quantities that show different values in different phase-like forms of the material can be used as order parameters, and ideally one could define suitable restricted thermodynamic potentials in terms of such an order parameter that distinguishes the phases. The restricted thermodynamic potential in terms of these parameters would exhibit a double minimum potential over some finite range of temperature or total energy;[110] this would identify the slush state with the coexistence region. Our system does not appear to behave like an ideal system, but that framework does provide a starting point for further analysis of the finite analogs of first-order bulk phase transitions. Our current understanding is less quantitative; however, by analyzing results for large particles, we developed the following definitions for the solid, liquid, and slush states of clusters and nanoparticles: A solid state is the state in which the properties c, β, and $\ln \kappa$ increase almost linearly with temperature. A solid state often has small volume and radius, and these properties are smooth functions of temperature. (1) A liquid state is the state in which c decreases linearly with temperature, β linearly increases with temperature or is close to constant, and $\ln \phi$ increases linearly with temperature. A liquid state often has large volume and radius, and these properties are smooth functions of temperature. (2) A slush state is between the solid state and liquid states, and one or more of the three properties is not a smooth function of temperature.

Applying the above definitions of the solid, liquid, and slush states to all the particles we studied, T_f and T_m can be roughly determined. The results are listed in Table 1. The T_p values for each property are also listed, where a value in parentheses indicates a deep valley. The T_p values of $\ln \kappa$ for those particles without sharp peaks but just jumps or drops are determined as the peak or valley positions of $d \ln \kappa/dT$. The T_f and T_m values listed are all determined by drawing straight lines in the c, β, and $\ln \kappa$ plots as we have done for Al_{300} since it is hard to determine these points as unambiguously as one can determine the peak temperature T_p of c. Consequently, the T_f and T_m values listed in the table have large uncertainties due to the fact that phase transitions in finite systems occur in a broad coexistence region, and there is no freezing or melting *point* in finite systems.[11] Of course, the values also involve uncertainties due to the inexactness of the potential-energy function and neglect of excited electronic states, but quantitative estimates of those uncertainties must await further studies.

The T_f and T_m values in Table 1 can be used to ascertain whether a particle is in a solid, slush, or liquid state at a given temperature: solid at temperatures below T_f, liquid at temperatures above T_m, and slush at temperatures between T_f and T_m. Many particles can be viewed as slush even at room temperature; these are marked with asterisks in Table 1. However, the melting of nanoparticles is different from that of macroscopic systems which are composed of separated solid and liquid spatial domains (like ice and water) in the coexistence region. For nanoparticles, in the coexistence region (i.e., in the slush state), the solid-like and liquid-like structures are in rapid equilibrium with each other.[9,11−13,15,17,18,41] From the $P(0)$ values given in the Supporting Information as a function of temperature, it is possible to roughly identify how many solid-like structures contribute to the slush state at a given temperature between T_f and T_m.

(110) Wales, D. J.; Berry, R. S. *Phys. Rev. Lett.* **1994**, *73*, 2875. Wales, D. J. *Energy Landscapes*; Cambridge University Press: Cambridge, 2003; pp 440−452.

Since many isomers with solid-like and liquid-like properties are in equilibrium with each other[9,11−13] in the coexistence region, depending on the sensitivity of the investigated property to the structural change (or isomerization) process, T_p values for different properties can be very different. For many particles, there are even multiple peaks. However, for particles having a single sharp peak in each property, the three peaks usually have the same T_p value. For example, for Al_{300}, the three peaks are at 709, 717, and 700 K for c, β, and $\ln \kappa$, respectively. For Al_{55}, the three peaks are at 667, 678, and 680 K for c, β, and $\ln \kappa$, respectively. For these particles, it is still useful to use the peak temperature of c to characterize the melting transitions. However, one must bear in mind that since $T_f \neq T_m$ for finite systems, comparing the peak temperature of a property, such as the T_p determined from the c curve, to the melting point of the bulk material may not be meaningful.

Table 1 indicates that most large particles (nanoparticles under our definition given at the end of the Introduction) have T_m values, i.e., the slush to liquid-state change temperatures, around 900−1000 K, a temperature range close to the bulk[103] melting temperature of 933 K. Plots of c (Figure 4d), β (Figure S-8 in the Supporting Information), and $\ln \kappa$ (Figure S-11 in the Supporting Information) also indicate that for most particles the three properties have similar linear temperature dependences above 900−1000 K. Since nanoparticles become quasispherical (prolate[91]) droplets above T_m, atoms and valence electrons in the droplets can be viewed as free particles constrained in a sphere.[1,111] Therefore, these liquid droplets may have similar properties.

To further confirm that T_m is approximately in the 900−1000 K temperature range for Al nanoparticles, in Figure 15 we plotted $P(E)$ for Al_{70} and Al_{130}. Both plots indicate that after 1000 K the distribution of the isomers does not change much; for Al_{70}, the peak of the distribution remains at about 2 eV and that of Al_{130} remains at about 5 eV. The $P(E)$ vs T curves in the temperature range of coexistence are significantly different from one temperature to the next, indicating that the change of temperature changes the distribution more dramatically in the slush state than at temperatures above the coexistence region. Therefore, above 1000 K, the particle may be viewed as in one single state, the liquid state. The plots also clearly indicate that for nanoparticles there is no clear border between solid, slush, and liquid states. For example, for Al_{70}, the populations of the isomers that are dominant at 500 K, a temperature lower than the highest T_p of c (565 K) which is defined as the melting temperature by most studies, are still non-negligible above 1000 K.

Table 1 indicates that smaller particles have higher T_m. Under our definition of the liquid state, many of the small clusters (Al_{12}, Al_{13}, $Al_{15}-Al_{17}$) have no liquid state. For $Al_{14}-Al_{17}$, they do not have a solid state in the temperature range we studied. As emphasized above, it is more appropriate to say that Al_n clusters (i.e., Al_n with $n \leq 18$) have no melting *transition* at all.

5. Concluding Remarks

Previously the melting transitions of finite-size systems have been widely studied for model systems. Here we investigated the melting transition of metal nanoparticles with a realistic many-body potential developed previously from quantum mechanical calculations on nanoparticles. In particular, we carried
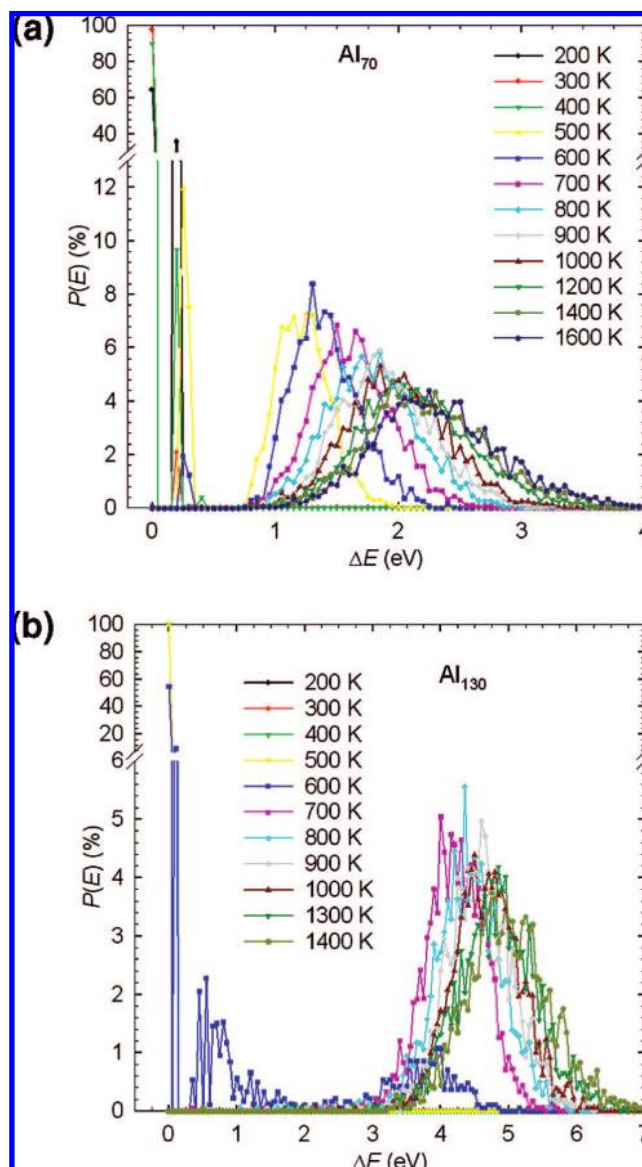
(111) Brack, M. *Rev. Mod. Phys.* **1993**, *65*, 677.

Figure 15. Percentage ($P(E)$) of quenched structures in a potential-energy range between E and $E + \delta E$ with $\delta E = 0.05$ eV: (a) Al_{70} and (b) Al_{130}. The abscissa is the potential energy relative to the global minimum structure.

out and analyzed molecular dynamics simulations of Al_n clusters and nanoparticles for a wide range of temperatures and n. The heat capacity, radius of gyration, volume, thermal coefficient of expansion, isothermal compressibility, and potential-energy distribution of the quenched structures were found to be informative of equilibrium phase behavior and therefore used as the basis of our investigations.

Analyzing the results for Al_n implies that the slush state previously characterized for model systems (with pairwise potentials) by Berry and co-workers[9−12] also exists for real metal nanoparticles. Analysis of the nanoparticle properties as a function of temperature gives new insight into the character of the phases (also called states, i.e., liquid state, solid state, etc.) even at room temperature, where we find that many nanoparticles are slushes (others being solids). This understanding contributes to the theoretical foundation for the design of metal quantum dots with tunable properties. Our analysis led to new operational definitions of the solid, slush, and liquid states in metal clusters and nanoparticles based on the temperature

dependence of heat capacity, thermal coefficient of expansion, and logarithm of isothermal compressibility. Applying the definitions, the freezing temperatures (T_f) and melting temperatures (T_m) for various sizes of aluminum particles have been estimated and can be used to identify the state of a particle at given temperatures; in particular, the particle is in the solid, slush, and liquid states at temperatures below T_f, between T_f and T_m, and above T_m. For most nanoparticles the liquid state is above 900−1000 K. Below that is the coexistence region, which may be called the slush state. At the low temperature end of the coexistence region is the solid state. Some particles have no solid state in the temperature range we studied at all, and many particles can be viewed as slush even at room temperature.

By careful examination of various physical properties of the particles and the potential-energy distributions of the quenched intermediate configurations during the melting simulations, we showed that it is more appropriate to say that clusters, defined here as particles less than about 1 nm in diameter, in particular Al_{18} and smaller, have no melting transition and are best understood as isomerizing molecules. On the other hand, aluminum nanoparticles, defined here as particles larger than about 1 nm in diameter, that is, Al_{19} and larger, exhibit melting behavior as in macroscopic systems. (It is just an accident that the 1 nm size border, which is used as our somewhat arbitrary border between clusters and nanoparticles, coincides so closely with the border in behavior ($n \leq 18$ vs $n \geq 19$). One must bear in mind that there is arbitrariness in the border between molecule-like particles (clusters) and nanoparticles that exhibit macroscopic-like melting behavior. For example, for Al_{19}−Al_{25}, the GM structure is still non-negligible above 1600 K ($P(0) >$ 5 at 1600 K). Unlike macroscopic systems, nanoparticles have a large temperature window of coexistence between the solid and liquid state.[1−18,25,37,41] In the solid−liquid coexistence region, i.e., in the slush state, although the peaks in the three physical properties used to distinguish solid from liquid states have finite widths, the peaks associated with the properties may not overlap or these properties may have no sharp peak at all or some properties may have multiple peaks such that there is no unambiguous transition temperature.

Supporting Information Available: Plots of heat capacity, radius of gyration, volume, coefficient of thermal expansion, compressibility, and $P(0)$ (the percentage in all the quenched structures of structures not higher than the GM structure by 0.05 eV) for all particles as a function of temperature. This material is available free of charge via the Internet at http://pubs.acs.org.

JA802389D